Inorganic Chemistry

Article

Group IV Imino-Semiquinone Complexes Obtained by Oxidative Addition of Halogens

Karen J. Blackmore, Michael B. Sly, Mason R. Haneline, Joseph W. Ziller, and Alan F. Heyduk*

Department of Chemistry, University of California, Irvine, California 92697

An isostructural series of titanium, zirconium, and hafnium complexes, M[ap]$_2$L$_2$ (M = Ti, Zr, Hf; L = THF, pyridine), of the redox-active 4,6-di-*tert*-butyl-2-*tert*-butylamidophenolate ligand ([ap]$^{2-}$) have been prepared. The zirconium and hafnium derivatives react readily with halogen oxidants such as XeF$_2$, PhICl$_2$, and Br$_2$, leading to products in which one-electron oxidation of each [ap]$^{2-}$ ligand accompanies halide addition to the metal center. Iodine proved to be too weak of an oxidant to yield the corresponding oxidative addition product, and under no conditions could halogen oxidative addition products be obtained for titanium. According to X-ray crystallographic studies, the zirconium and hafnium oxidation products are best formulated as MX$_2$[isq·]$_2$ ([isq·]$^-$ = 4,6-di-*tert*-butyl-2-*tert*-butylimino-semiquinonate; M = Zr, Hf; X = F, Cl, Br) species, in which the molecule is symmetric with each redox-active ligand in the semiquinone oxidation state. Temperature-dependent magnetization measurements suggest a singlet ($S = 0$) ground-state for the diradical complexes with a thermally accessible triplet ($S = 1$) excited state. Solution electron paramagnetic resonance (EPR) spectra are consistent with this assignment, showing both $\Delta m_s = 1$ and $\Delta m_s = 2$ transitions for the antiferromagnetically coupled electrons.

Introduction

Redox-active *ortho*-aminophenols have attracted considerable interest as ligands for transition- and main-group metal complexes for their ability to become involved with electronic properties normally associated with the metal valence electrons. Early studies of nickel complexes highlighted the complications associated with assigning the oxidation state of metal complexes of noninnocent ligands.[1–5] Subsequent spectroscopic and theoretical analyses have further illustrated the importance of considering the valence electron distribution of the entire metal complex when examining oxidation and reduction reactions in which both the metal and ligands are redox-active.[6–9] Similarly, the extent of metal–ligand orbital mixing varies with the donor atoms,[10,11] and the reduction potentials of coordinated quinone-type ligands are tunable over a wide range by simply replacing the oxygen donors with nitrogen donor groups.[12]

The interplay of ligand- and metal-based electronic properties offers intriguing possibilities for the design of new multielectron reagents. Redox-active, amidophenolate ligands have been incorporated into copper catalysts to mimic the galactose oxidase aerobic oxidation of primary alcohols.[13,14] Catecholate complexes of manganese and other midtransition metals catalyze the oxidation of catechols to *ortho*-quinones with molecular oxygen.[15–17] These examples hint at the

* To whom correspondence should be addressed. E-mail: aheyduk@uci.edu.

(1) Schauzer, G. N.; Mayweg, V. P. *J. Am. Chem. Soc.* **1965**, *87*, 1483–1489.
(2) Steifel, E. I.; Waters, J. H.; Billig, E.; Gray, H. B. *J. Am. Chem. Soc.* **1965**, *87*, 3016–3017.
(3) Balch, A. L.; Holm, R. H. *J. Am. Chem. Soc.* **1966**, *88*, 5201–5209.
(4) Swartz Hall, G.; Soderberg, R. H. *Inorg. Chem.* **1968**, *7*, 2300–2303.
(5) McCleverty, J. A. *Prog. Inorg. Chem.* **1968**, *10*, 49–221.
(6) Lim, B. S.; Fomitchev, D. V.; Holm, R. H. *Inorg. Chem.* **2001**, *40*, 4257–4262.
(7) Chun, H.; Verani, C. N.; Chaudhuri, P.; Bothe, E.; Bill, E.; Weyhermüller, T.; Wieghardt, K. *Inorg. Chem.* **2001**, *40*, 4157–4166.

(8) Sun, X.; Chun, H.; Hildenbrand, K.; Bothe, E.; Weyhermüller, T.; Neese, F.; Wieghardt, K. *Inorg. Chem.* **2002**, *41*, 4295–4303.
(9) Kokatam, S.; Weyhermüller, T.; Bothe, E.; Chaudhuri, P.; Wieghardt, K. *Inorg. Chem.* **2005**, *44*, 3709–3717.
(10) Pierpont, C. G. *Coord. Chem. Rev.* **2001**, *216–217*, 99–125.
(11) Gorelsky, S. I.; Dodsworth, E. S.; Lever, A. B. P.; Vlcek, A. A. *Coord. Chem. Rev.* **1998**, *174*, 469–494.
(12) Masui, H.; Lever, A. B. P.; Auburn, P. R. *Inorg. Chem.* **1991**, *30*, 2402–2410.
(13) Chaudhuri, P.; Hess, M.; Müller, J.; Hildenbrand, K.; Bill, E.; Weyhermüller, T.; Wieghardt, K. *J. Am. Chem. Soc.* **1999**, *121*, 9599–9610.
(14) Wang, Y. D.; DuBois, J. L.; Hedman, B.; Hodgson, K. O.; Stack, T. D. P. *Science* **1998**, *279*, 537–540.
(15) Rolle, C. J.; Hardcastle, K. I.; Soper, J. D. *Inorg. Chem.* **2008**, *47*, 1892–1894.

utility of ligand-based redox properties in reaction chemistry, but still utilize mid- and late-transition metals where the assignment of redox changes to the ligand or metal can be ambiguous. We are interested in using redox-active ligands in coordination complexes of high-valent, early transition metals where amidophenolate ligands offer the opportunity for new multielectron reactivity through the participation of ligand-based redox changes. Despite this potential for new reactivity, the synthesis and study of Group IV metal complexes with redox-active ligands have been underdeveloped.[18,19]

Herein we report on the synthesis, characterization, and oxidative-addition reactivity of Group IV complexes with redox-active 4,6-di-*tert*-butyl-2-*tert*-butylamidophenolate ([ap]$^{2-}$) ligands. An isostructural series of metal complexes, M[ap]$_2$L$_2$ (M = Ti, Zr, Hf; L = THF, pyridine), were obtained and are best described as pseudo-octahedral, d^0 M^{IV} complexes. Upon exposure to halogen-based oxidants, the zirconium and hafnium derivatives react readily to give products formulated as MX$_2$[isq$\cdot$]$_2$ ([isq$\cdot$]$^-$ = 4,6-di-*tert*-butyl-2-*tert*-butylimino-semiquinonate; M = Zr, Hf; X = F, Cl, Br) formed by halide addition to the d^0 metal center with concomitant oxidation at the redox-active ligand. These complexes again are isostructural and isoelectronic with diradical electron configurations characterized by singlet (S = 0) ground states and a low-energy triplet (S = 1) excited states. Portions of this work have been reported previously.[20]

Experimental Procedures

Synthetic Considerations. The complexes described below are extremely air- and moisture-sensitive. All manipulations were carried out under an atmosphere of argon or nitrogen gas using standard Schlenk, vacuum-line, and glovebox techniques. High-purity solvents initially were sparged with argon and then passed through activated alumina and Q5 columns to remove water and oxygen, respectively. The metal salts ZrCl$_4$, and HfCl$_4$ were purchased from Alfa-Aesar and used as received. Ferrocenium hexafluorophosphate (Aldrich) and xenon difluoride (Aldrich) were used as received. Bromine (Acros) and iodine (EM Science) were purified by distillation from P$_2$O$_5$ and by sublimation, respectively. Dichloroiodobenzene[21] and TiCl$_4$(THF)$_2$[22] were prepared by the published procedures. The 4,6-di-*tert*-butyl-2-(*tert*-butylamino)phenol ([ap]H$_2$) and 4,6-di-*tert*-butyl-2-*tert*-butyliminoquinone (iq) ligands,[23] and the metal complexes Zr[ap]$_2$(THF)$_2$ (**1a**) and ZrCl$_2$[isq$\cdot$]$_2$ (**3b**),[20] were prepared by previously reported procedures.

General Methods. All complexes were characterized by ^{1}H and ^{13}C NMR spectroscopy, IR spectroscopy, and elemental analysis. NMR spectra were collected on Bruker Avance 500 or 600 MHz spectrometers in either benzene-d_6 or THF-d_8 solvents that were

degassed by several freeze−pump−thaw cycles, dried over sodium benzophenone-ketyl radical, and vacuum-distilled before use. ^{1}H and ^{13}C NMR spectra were referenced to TMS using the residual ^{1}H and natural abundance ^{13}C impurities of the solvent. All chemical shift values are reported using the standard δ notation in parts-per-million. Infrared spectra (450−4000 cm^{-1}) were recorded on a Perkin-Elmer Spectrum One spectrophotometer as KBr pellets. UV−vis absorbance spectra (270−900 nm) were recorded on a Perkin-Elmer Lambda 800 double-beam spectrophotometer equipped with a PMT detector. EPR spectra were collected on a Bruker EMX X-band spectrometer equipped with an ER041XG microwave bridge. Spectra for EPR samples were collected using the following spectrometer settings: attenuation = 25 dB, microwave power = 0.638 mW, frequency = 9.47 GHz, sweep width = 5000 G, modulation amplitude = 10.02 G, gain = 1.00 × 10^3, conversion time = 81.920 ms, time constant = 655.36 ms, and resolution = 1024 points. Solid-state magnetization measurements were recorded on a Quantum Design SQUID magnetometer at 10 kOe between 5 and 300 K using microcrystalline samples contained within a plastic capsule. Magnetic susceptibility data were corrected for background and underlying diamagnetic contributions by use of tabulated Pascal constants.[24] Schwarzkopf Microanalytical Laboratory and Desert Analytics provided elemental analyses.

Synthesis of Zr[ap]$_2$(py)$_2$ (1b). Complex **1b** was prepared by a procedure analogous to that reported for the synthesis of **1a**.[20] A frozen diethyl ether solution of [ap]Li$_2$, generated from 1.00 g of apH$_2$ (3.6 mmol) and 2 equiv of *n*BuLi in hexanes, was thawed and solid ZrCl$_4$ (0.42 g, 1.8 mmol) was added followed by 1 mL of pyridine. The reaction mixture was allowed to warm to 25 °C, during which time the color changed from yellow to red. The volatiles were removed *in vacuo* and the solid residue was triturated with pentane (2 × 10 mL). The product was then dissolved in toluene (15 mL) and filtered to removed LiCl. Removal of the toluene afforded **1b** as a red microcrystalline solid. Yield 553 mg (77%). ^{1}H NMR (500 MHz, C$_6$D$_6$) δ/ppm: 1.42 (*s*, 18H, C(C*H$_3$*)$_3$), 1.65 (*s*, 18H, C(C*H$_3$*)$_3$), 1.68 (*s*, 18H, C(C*H$_3$*)$_3$), 6.21 (*apparent triplet*, 4H, pyr,$^3J_{HH}$ = 7.0), 6.57 (*t*, 2H, pyr, $^3J_{HH}$ = 7.5), 6.99 (*d*, 2H, Ar-*H*, $^3J_{HH}$ = 2.0), 7.05 (*d*, 2H, Ar-*H*, $^4J_{HH}$ = 2.0), 9.09 (*d*, 2H, pyr, $^4J_{HH}$ = 4.5).

Synthesis of [Zr[ap]$_2$]$_2$ (2). A frozen diethyl ether solution of [ap]Li$_2$, generated from 0.5 g of apH$_2$ (1.8 mmol) and 2 equiv of *n*BuLi in hexanes, was thawed and solid ZrCl$_4$ (0.21 g, 0.9 mmol) was added. The reaction mixture was allowed to warm to 26 °C and then was stirred for 1 h. A white precipitate formed. Pentane (5 mL) was added and the precipitate was removed by filtration and washed with pentane. The reaction solution and filtrate washings were combined, and the solvent was removed under reduced pressure. The residue was very soluble in even small amounts of pentane, but one time a few X-ray quality crystals were obtained from slow evaporation of pentane solutions at −35 °C.

Synthesis of ZrF$_2$[isq$\cdot$]$_2$ (3a), Method A. A 0.5 g sample of **1b** (0.6 mmol) was dissolved in 8 mL of diethyl ether in a scintillation vial and the solution was frozen in a liquid nitrogen cold well. Upon removal from the cold well, the solution thawed and solid XeF$_2$ (0.1 g, 0.6 mmol) was added resulting in an immediate color change to green. The reaction mixture was shaken until all the reagents were dissolved at which point the vial was placed in the freezer and stored overnight at −35 °C. A dark green precipitate was separated from the cold solution and this solid was dried under vacuum to yield **3a** (0.05 g, 12% yield). IR (KBr) ν/cm^{-1}: 481, 518, 544, 578, 643, 658, 736, 748, 782, 811, 835,

(16) Hitomi, Y.; o, A.; Matsui, H.; Ito, T.; Tanaka, T.; Ogo, S.; Funabili, T. *Inorg. Chem.* **2005**, *44*, 3473–3478.

(17) Cass, M. E.; Pierpont, C. G. *Inorg. Chem.* **1986**, *25*, 122–123.

(18) Zanello, P.; Corsini, M. *Coord. Chem. Rev.* **2006**, *250*, 2000–2022.

(19) Pierpont, C. G.; Lange, C. W. *Prog. Inorg. Chem.* **1994**, *41*, 331–442.

(20) Blackmore, K. J.; Ziller, J. W.; Heyduk, A. F. *Inorg. Chem.* **2005**, *44*, 5559–5561.

(21) Lucas, H. J.; Kennedy, E. R. *Org. Synth.* **1955**, *3*, 482.

(22) Manzer, L. E. *Inorg. Synth.* **1982**, *21*, 135–140.

(23) Carter, S. M.; Sia, A.; Shaw, M. J.; Heyduk, A. F. *J. Am. Chem. Soc.* **2008**, *130*, 5838–5839.

(24) O'Connor, C. J. *Prog. Inorg. Chem.* **1982**, *29*, 203–283.

850, 880, 915, 946, 967, 1032, 1064, 1123, 1165, 1201, 1217, 1237, 1257, 1304, 1361, 1395, 1415, 1479, 1599, 2870, 2906, 2962. UV–vis (CCl$_4$) λ_{max}/nm (ε/M^{-1} cm^{-1}): 803 (886).

Method B. A pentane solution of **1b** (0.10 g, 0.13 mmol) and ferrocenium hexafluorophosphate (62 mg, 0.13 mmol) was stirred overnight and turned from red to green. The volatiles were removed and ferrocene and C$_5$H$_5$N-PF$_5$ were removed by vacuum sublimation at 130 °C and 0.1 mtorr. Yield 82 mg (82%).

Synthesis of ZrCl$_2$[isq·]$_2$ (3b) from isqLi. A 10-mL diethyl ether solution of [ap]Li$_2$ derived from 50 mg of apH$_2$ (0.19 mmol) was treated with 50 mg of iq (0.19 mmol) resulting in an immediate color change to forest green. The solution was frozen and then thawed. Solid ZrCl$_4$ (45 mg, 0.19 mmol) was added to the cold solution. The mixture was stirred for 10 min and then placed in a −35 °C freezer overnight. Dark green, microcrystalline **3b** was isolated from the green supernatant solution in 62% yield (90 mg).

Synthesis of ZrBr$_2$[isq·]$_2$ (3c). A diethyl ether solution of **1a** (0.5 g, 0.6 mmol) was frozen in a liquid nitrogen cold well. The frozen solution was removed from the cold well, thawed, and Br$_2$ (33 μL, 0.6 mmol) was added. The reaction mixture was shaken and then placed in a −35 °C freezer overnight. Decanting the supernatant solution gave the dark green product, **3c** (0.261 g, 51% yield) Anal. Calcd. for C$_{36}$H$_{58}$Br$_2$N$_2$O$_2$Zr: C, 53.92; H, 7.29; N, 3.49. Found: C, 52.82: H, 7.14; N, 3.31. IR (KBr) ν/cm^{-1}: 484, 499, 511, 548, 613, 644, 678, 772, 832, 856, 888, 914, 1006, 1025, 1045, 1116, 1199, 1224, 1247, 1267, 1307, 1320, 1363, 1392, 1408, 1437, 1460, 1478, 1516, 1529, 1579, 1626, 2869, 2963. UV–vis (C$_6$H$_6$) λ_{max}/nm (ε/M^{-1} cm^{-1}): 797 (6311).

Synthesis of Ti[ap]$_2$(THF)$_2$ (4). Complex **4** was prepared by a procedure analogous to that reported for the synthesis of **1a**.[20] In a 20 mL vial, apH$_2$ (0.50 g, 1.8 mmol) dissolved in 10 mL of diethyl ether was deprotonated with n-butyllithium (1.4 mL, 3.6 mmol). The solution was then frozen in a liquid nitrogen cold well. The solution was removed from the cold well and allowed to thaw before TiCl$_4$(THF)$_2$ (0.30 g, 0.70 mmol) was added. Upon warming of the solution to 26 °C, a white precipitate formed, which was removed by filtration. The product **4a** was obtained in 74% yield (1.0 g) after solvent removal. X-ray quality crystals were obtained from a chilled ether solution. Anal. Calcd. for C$_{44}$H$_{74}$N$_2$O$_4$Ti: C, 71.13; H, 10.04; N, 3.77. Found: C, 70.74: H, 7.95; N, 4.04. ^{1}H NMR (500 MHz, C$_6$D$_6$) δ/ppm: 1.15 (m, 8H, THF), 1.38 (s, 18H, C(CH$_3$)$_3$), 1.56 (s, 18H, C(CH$_3$)$_3$), 1.72 (s, 18H, C(CH$_3$)$_3$), 3.88 (m, 8H, THF), 6.87 (d, 2H, Ar-H, ^{4}J$_{HH}$ = 2.0), 6.95 (d, 2H, Ar-H, ^{4}J$_{HH}$ = 2.0). ^{13}C NMR (125.8 MHz, C$_6$D$_6$) δ/ppm: 25.1 (THF), 30.5 (C(CH$_3$)$_3$), 31.5 (C(CH$_3$)$_3$), 32.3 (C(CH$_3$)$_3$), 34.8 (C(CH$_3$)$_3$), 60.3 (C(CH$_3$)$_3$), 71.5 (THF), 110.1 (Ar-C), 113.5 (Ar-C), 131.9 (Ar-C), 140.4 (Ar-C), 149.7 (Ar-C), 151.5 (Ar-C). IR (KBr) ν/cm^{-1}: 459, 478, 499, 541, 565, 647, 669, 690, 746, 784, 813, 832, 852, 879, 897, 916, 967, 1003, 1036, 1120, 1166, 1198, 1263, 1303, 1361, 1390, 1413, 1458, 1482, 2868, 2960, 3263. UV–vis (C$_6$H$_6$) λ_{max}/nm (ε/M^{-1} cm^{-1}): 371 (11500).

Synthesis of Hf[ap]$_2$(THF)$_2$ (5). Complex **5** was prepared by a procedure analogous to that used for the synthesis of **1a** and **4a** from 0.58 g of apH$_2$ (2.1 mmol), 2 equiv of nBuLi, and 0.50 g of HfCl$_4$(THF)$_2$ (1.05 mmol). **5** was obtained as an off-white micro-crystalline solid (0.7608 g, 83% yield). X-ray quality crystals were obtained from chilled ether solutions. Anal. Calcd. for C$_{44}$H$_{74}$N$_2$O$_4$Hf: C, 60.5; H, 8.54; N, 3.21. Found: C, 58.20: H, 8.05; N, 3.10. ^{1}H NMR (500 MHz, C$_6$D$_6$) δ/ppm: 1.10 (m, 8H, THF), 1.41 (s, 18H, C(CH$_3$)$_3$), 1.63 (s, 18H, C(CH$_3$)$_3$), 1.64 (s, 18H, C(CH$_3$)$_3$), 3.75 (m, 4H, THF), 4.07 (m, 4H, THF), 6.92 (d, 2H, Ar-H, ^{4}J$_{HH}$ = 2.0), 6.99 (d, 2H, Ar-H, ^{4}J$_{HH}$ = 2.5). ^{13}C NMR (125.8 MHz, C$_6$D$_6$) δ/ppm: 25.0 (THF), 30.5 (C(CH$_3$)$_3$), 30.9 (C(CH$_3$)$_3$),

32.5 (C(CH$_3$)$_3$), 34.8 (C(CH$_3$)$_3$), 53.8 (C(CH$_3$)$_3$), 73.4 (THF), 110.7 (Ar-C), 112.2 (Ar-C), 133.1 (Ar-C), 139.4 (Ar-C), 148.5 (Ar-C), 151.3 (Ar-C). IR (KBr) ν/cm^{-1}: 455, 485, 507, 560, 641, 656, 681, 738, 771, 785, 828, 867, 903, 920, 962, 1007, 1035, 1071, 1121, 1131, 1200, 1238, 1266, 1303, 1324, 1360, 1388, 1416, 1436, 1465, 1560, 2868, 2962, 3252. UV–vis (C$_6$H$_6$) λ_{max}/nm (ε/M^{-1} cm^{-1}): 322 (10500).

Synthesis of HfCl$_2$[isq·]$_2$ (6b). Complex **6b** was prepared by a procedure analogous to that used for the synthesis of **3a−c** using 0.50 g of **5** (0.63 mmol) and 0.175 g of PhICl$_2$ (0.63 mmol). The product was isolated as a dark-green, microcrystalline solid in 55% yield (0.25 g). Anal. Calcd. for C$_{36}$H$_{58}$Cl$_2$N$_2$O$_2$Hf: C, 54.03; H, 7.31; N, 3.50. Found: C, 54.03: H, 7.09; N, 3.41. IR (KBr) ν/cm^{-1}: 484, 669, 801, 831, 889, 987, 1027, 1201, 1245, 1273, 1302, 1363, 1376, 1399, 1418, 1459, 1480, 1508, 1542, 1559, 1578, 1627, 1650, 1663, 1705, 1717, 1749, 2965. UV–vis (CCl$_4$) λ_{max}/nm (ε/M^{-1} cm^{-1}): 760 (4362).

Synthesis of HfBr$_2$[isq·]$_2$ (6c). Complex **6c** was prepared by a procedure analogous to that used for the synthesis of **3a−c** using 0.5 g of **5** (0.64 mmol) and 34 μL of Br$_2$ (0.64 mmol). The product was isolated as a dark-green, microcrystalline solid in 61% yield (0.31 g). Anal. Calcd. for C$_{36}$H$_{58}$Br$_2$N$_2$O$_2$Hf: C, 48.63; H, 6.57; N, 3.15. Found: C, 48.80: H, 6.58; N, 3.04. IR (KBr) ν/cm^{-1}: 501, 644, 680, 832, 857, 889, 1045, 1199, 1246, 1272, 1306, 1363, 1396, 1459, 1480, 1508, 1542, 1559, 1626, 1650, 1663, 1682, 1717, 1749, 2963. UV–vis (CCl$_4$) λ_{max}/nm (ε/M^{-1} cm^{-1}): 765 (4887).

Crystallographic Procedures. X-ray diffraction data were collected on crystals mounted on glass fibers using a Bruker CCD platform diffractometer equipped with a CCD detector. Measurements were carried out at 163 K using Mo Kα (λ = 0.71073 Å) radiation, which was wavelength selected with a single-crystal graphite monochromator. The SMART program package was used to determine unit-cell parameters and to collect data.[25] The raw frame data were processed using SAINT[26] and SADABS[27] to yield the reflection data files. Subsequent calculations were carried out using the SHELXTL[28] program suite. Structures were solved by direct methods and refined on F^2 by full-matrix least-squares techniques. Analytical scattering factors for neutral atoms were used throughout the analyses.[29] Hydrogen atoms were included using a riding model. ORTEP diagrams were generated using ORTEP-3 for Windows.[30] Diffraction data are shown in Table 1.

Results

Synthesis and Characterization of Group 4 Complexes of [ap]$^{2-}$. Group 4 metals readily bind 2 equiv of the chelating dianionic ligand [ap]$^{2-}$ and two neutral donor ligands to form neutral six-coordinate complexes. In the case of the smaller catecholate ligands, the Group IV coordination chemistry is dominated by the very stable homoleptic [M(cat)$_3$]$^{2-}$ dianions.[31,32] The titanium complex Ti[ap]$_2$-

(25) SMART Software Users Guide, Version 5.1; Bruker Analytical X-Ray Systems, Inc.: Madison, WI 1999.
(26) SAINT Software Users Guide, Version 6.0; Bruker Analytical X-Ray Systems, Inc.: Madison, WI 1999.
(27) Sheldrick, G. M. SADABS, Version 2.10; Bruker Analytical X-Ray Systems, Inc.: Madison, WI 2002.
(28) Sheldrick, G. M. SHELXTL Version 6.12; Bruker Analytical X-Ray Systems, Inc.: Madison, WI 2001.
(29) *International Tables for X-Ray Crystallography*; Kluwer Academic Publishers: Dordrecht, 1992; Vol. *C*.
(30) Farrugia. L. J. *J. Appl. Crystallogr.* **1997**, *30*, 565.
(31) Rosenheim, A.; Sorge, O. *Chem. Ber.* **1920**, *53B*, 932–939.
(32) Borgias, B. A.; Cooper, S. R.; Koh, Y. B.; Raymond, K. N. *Inorg. Chem.* **1984**, *23*, 1009–1016.

Table 1. X-ray Diffraction Data-Collection and Refinement Parameters

	[Zr[ap]₂]₂ (**2**)	ZrBr₂[isq·]₂ (**3c**)	Ti[ap]₂(THF)₂ (**4**)	Hf[ap]₂(THF)₂ (**5**)	HfCl₂[isq·]₂ (**6b**)	HfBr₂[isq·]₂ (**6c**)
empirical formula	C₇₂H₁₁₆N₄O₄Zr₂	C₃₆H₅₈Br₂N₂O₂Zr	C₄₄H₇₄N₂O₄Ti·C₄H₈O	C₄₄H₇₄HfN₂O₄·C₄H₁₀O	C₃₆H₅₈Cl₂HfN₂O₂	C₃₆H₅₈Br₂N₂O₂Hf
formula weight	1284.13	801.88	815.06	947.66	800.23	889.15
crystal system	triclinic	monoclinic	monoclinic	monoclinic	monoclinic	monoclinic
space group	P$\bar{1}$	C2/c	P2₁/c	P2₁/c	C2/c	C2/c
a/Å	11.5149(19)	21.367(2)	13.0935(15)	13.3201(14)	21.143(2)	21.351(10)
b/Å	14.213(2)	9.6659(10)	19.650(2)	19.716(2)	9.5596(9)	9.661(5)
c/Å	21.610(4)	18.6173(19)	19.141(2)	19.218(2)	18.7268(18)	18.668(9)
α/deg	88.275(4)	90	90	90	90	90
β/deg	85.543(3)	94.675(2)	102.249(2)	102.407(2)	94.765(2)	94.783(8)
γ/deg	79.574(3)	90	90	90	90	90
V/Å³	3467.4(10)	3832.2(7)	4812.5(10)	4929.3(9)	3772.0(6)	3837(3)
Z	2	4	4	4	4	4
refl collected	29975	20187	46305	50452	19066	20564
indep refl	11837	4564	9845	10887	4153	4709
R1	0.0653	0.0378	0.0589	0.0270	0.0336	0.0318
wR2	0.1615	0.0976	0.1456	0.0630	0.0620	0.0676

(THF)₂ (**4a**) was prepared by the addition of TiCl₄(THF)₂ to a cold ether solution of [ap]Li₂, as prepared in situ from apH₂ and 2 equiv of *n*BuLi. Complex **4** was isolated as a purple crystalline solid after removal of the LiCl byproduct followed by cooling a concentrated ether solution of the complex to −35 °C. Zirconium and hafnium analogues **1a** and **5**, respectively, could be prepared by analogous reactions; however, the reduced Lewis acidity of their base-free salts allowed direct metalation of MCl₄ without first forming the THF adduct. In the case of **1a** and **5**, the complexes were isolated as yellow crystalline solids. When metalation reactions were carried out with ZrCl₄ and in the presence of two or more equivalents of pyridine, the pyridine adduct, Zr[ap]₂(py)₂ (**1b**), was isolated rather than the THF adduct.

The solid-state structures of complexes **1a**, **4**, and **5** reveal isostructural coordination environments around each metal center. The solid-state structure of titanium derivative **4** is shown in Figure 1; the structures of zirconium and hafnium derivatives **1a** and **5**, respectively, can be found in the Supporting Information. Selected metrical parameters for all three derivatives can be found in Table 2. The coordination geometry about the metal center in complexes **1a**, **4**, and **5** is nearly octahedral with a distortion owing to the acute O−M−N angle enforced by the amidophenolate ligand (76−80°). The equatorial ligands are twisted 30° away from planar. In every case, the amidophenolate ligands coordinate such that the oxygen donors are located approximately *trans* to one another (∠OMO ≅ 160°), while the amide nitrogen

Table 2. Selected Metrical Data for M[ap]₂(THF)₂ (**1a**, M = Zr; **4**, M = Ti; **5**, M = Hf)

	Zr[ap]₂(THF)₂ (**1a**)	Ti[ap]₂(THF)₂ (**4**)	Hf[ap]₂(THF)₂ (**5**)
		bond lengths/Å	
M−O(1)	2.056(3)	1.9281(19)	2.047(2)
M−O(2)	2.057(3)	1.9297(19)	2.0456(19)
M−N(1)	2.128(4)	2.004(2)	2.117(2)
M−N(2)	2.124(4)	2.004(2)	2.117(2)
M−O(3)	2.276(3)	2.200(2)	2.254(2)
M−O(4)	2.289(3)	2.190(2)	2.261(2)
		bond angles/deg	
O(1)−M−N(1)	75.76(13)	79.97(9)	76.97(9)
O(1)−M−O(2)	159.89(12)	161.98(8)	159.64(8)
N(1)−M−N(2)	103.89(15)	100.36(10)	103.31(10)
O(3)−M−O(4)	84.14(12)	83.23(8)	83.72(8)
O(1)−M−O(3)	86.51(12)	87.39(8)	86.62(8)
N(1)−M−O(3)	89.67(13)	90.54(9)	89.78(9)

donors are located in *cis* coordination sites (∠NMN ≅ 104°). The alternative coordination mode, with a *trans* arrangement of the amide nitrogen donors, has not been observed, presumably to avoid competition between the amides for the same metal d orbitals in both the σ- and π-bonding manifolds.[33] The cis arrangement of the amide ligands avoids this competition and places the amides trans to the less basic THF molecules, which readily exchange in solution. As can be seen in Table 2, the M−O and M−N bond distances display the expected trends on moving down the Group from titanium to zirconium to hafnium.

In solution, rapid exchange occurs between the coordinated THF molecules of **1a**, **4**, and **5** and uncoordinated THF. Solution ¹H and ¹³C NMR spectra in benzene-*d₆* are consistent with the solid-state structures obtained from single-crystal diffraction experiments. For example, zirconium derivative **1a** displays five resonances for the coordinated [ap]²⁻ ligands, consistent with *C₂* symmetry in solution: three aliphatic singlets correspond to *tert*-butyl groups and two aromatic singlets correspond to aromatic protons at the 3- and 5-positions of the aromatic ring. In benzene-*d₆*, the coordinated THF molecules of zirconium derivative **1a** gave rise to diagnostic resonances at 1.40, 3.79, and 4.11 ppm; however, the ¹H NMR spectrum taken in THF-*d₈* showed these coordinated solvent molecules were readily displaced.

Figure 1. ORTEP diagrams of Ti[ap]₂(THF)₂ (**4**). Thermal ellipsoids are plotted at 50% probability. Hydrogen atoms and an uncoordinated THF molecule have been omitted for clarity.

(33) Burdett, J. K.; Albright, T. A. *Inorg. Chem.* **1979**, *18*, 2112−2120.
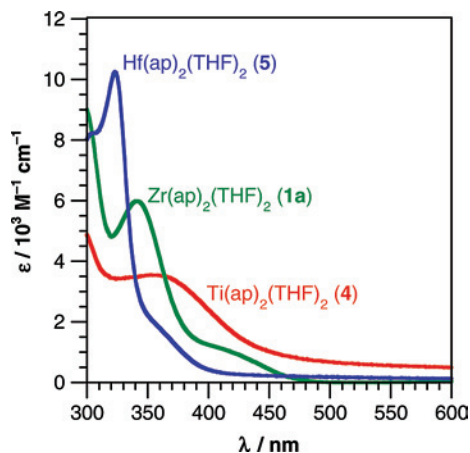
Figure 2. UV−vis absorbance spectra for M[ap]₂(THF)₂ (**1a**, M = Zr, green; **4**, M = Ti, red; **5**, M = Hf, blue) complexes recorded in benzene.

Figure 3. ORTEP diagram of {Zr[ap]₂}₂ (**2**). Thermal ellipsoids are plotted at 50% probability. Hydrogen atoms and select *tert*-butyl groups have been omitted for clarity.

The only significant differences observed in the NMR spectra of **1a**, **4**, and **5** corresponded to the geminal proton resonances of the coordinated THF ligands. In zirconium and hafnium complexes **1a** and **5**, two resonances are observed, whereas, in titanium complex **4**, the geminal protons of the THF molecules are equivalent, suggesting that THF exchange is fast on the NMR time scale.

The color differences observed between solutions of titanium derivative **4** and zirconium and hafnium derivatives **1a** and **5**, respectively, prompted an investigation of the solution absorbance spectra of the complexes. As shown in Figure 2, the UV−vis absorbance spectrum of hafnium complex **5** is dominated by a strong transition at 321 nm with a shoulder at 350 nm. A similar pattern is observed for zirconium complex **1a**, though the high-energy band is broadened considerably and red-shifted to 340 nm with the shoulder near 400 nm. Moving up the column to titanium derivative **4**, the high-energy peak is observed at 364 nm and is broadened to the point that it tails out well into the visible portion of the spectrum, but the shoulder is not readily visible. The energy and extinction coefficients for the absorbance bands of **1a**, **4**, and **5** suggest significant charge-transfer character. Furthermore, the formal d⁰ electron count for the metal centers and the progression of the absorption band to higher upon descending the triad suggests that these transitions are best assigned as ligand-to-metal charge-transfer (LMCT) transitions originating at the electron rich [ap]²⁻ ligands.[32] In the case of titanium derivative **4**, the transition is red-shifted relative to the LMCT transitions observed for other titanium(IV) amide and alkoxide derivatives. For example, the low-energy LMCT transition in titanium tetrakis(phenoxide), Ti(OPh)₄, is observed at approximately 345 nm and does not significantly absorb visible wavelengths of light.[34]

In an attempt to isolate a solvent-free zirconium-amidophenolate complex, the reaction of [ap]Li₂ with ZrCl₄ in the absence of THF, pyridine, or other two-electron donor ligands, was investigated. Reactions carried out in diethyl-

ether afforded the expected LiCl byproduct and the formation of a dark red, pentane-soluble metal complex identified by X-ray crystallography as {Zr[ap]₂}₂ (**2**). Whereas addition of THF to **2** afforded the readily characterized adduct **1a**, the ¹H and ¹³C NMR spectra of **2** were impossibly complex in benzene-*d₆*. Dark red crystals of **2** were obtained in low yields from solutions stored for several weeks at −35 °C. As shown in Figure 3, complex **2** is a dimer in which oxygen atoms of two [ap]²⁻ ligands bridge the zirconium centers. The formation of Group IV cluster complexes with bridging catecholate ligands is established.[35,36] Because of the intractability of **2**, further attempts to prepare solvent-free complexes of the [ap]²⁻ ligand were not pursued.
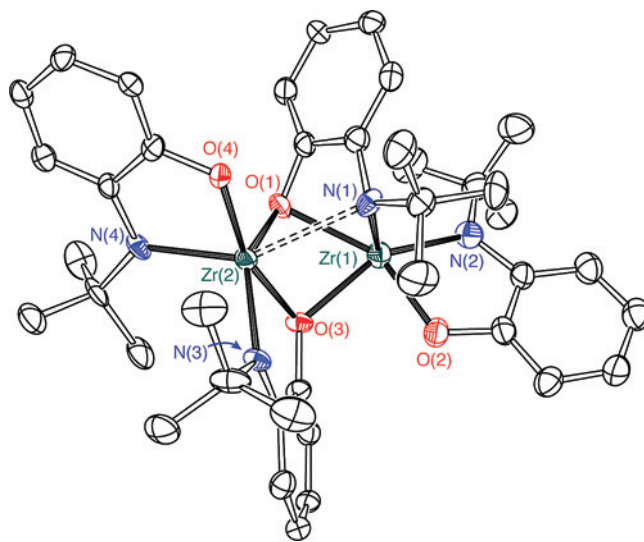
Oxidation Reactions of M[ap]₂L₂ Complexes. We have communicated that **1a** reacted rapidly with PhICl₂ to afford the oxidative addition product ZrCl₂[isq•]₂ (**3b**) as shown in Scheme 1.[20] Upon addition of the oxidant to a cold yellow solution of **1a**, an immediate color change to dark green was observed. To maximize the yield of **3b**, the reaction mixture was kept at −35 °C overnight. In this way, large dark green crystals of **3b** could be isolated in up to 55% yield. Complex **3b** was also generated by the reaction of elemental chlorine with **1a** at low temperature.

According to Scheme 1, other halogen-based oxidants reacted with **1a** to afford the halide products analogous to dichloride **3b**. Upon addition of elemental bromine to solutions of **1a**, a dark green color developed from which green crystalline ZrBr₂[isq•]₂ (**3c**) was isolated in 51% yield. The yield of this reaction is sensitive to the reaction temperature, with warmer temperatures significantly reducing the isolated yield of product. Other reagents that could be used as halogen equivalents were PCl₂Ph₃, PBr₂Ph₃, and ClCPh₃; however, in reactions carried out with these reagents it was impossible to separate completely the desired zirconium product from the PPh₃ or Ph₃CCPh₃ byproducts. The

(34) Dijkgraaf, C.; Rousseau, J. P. G. *Spectrochim. Acta, Part A* **1969**, *25*, 1831–1839.

(35) Wallace, W. A.; Potvin, P. G. *Inorg. Chem.* **2007**, *46*, 9463–9472.
(36) Boyle, T. J.; Tribby, L. J.; Alam, T. M.; Bunge, S. D.; Holland, G. P. *Polyhedron* **2005**, *24*, 1143–1152.

Scheme 1
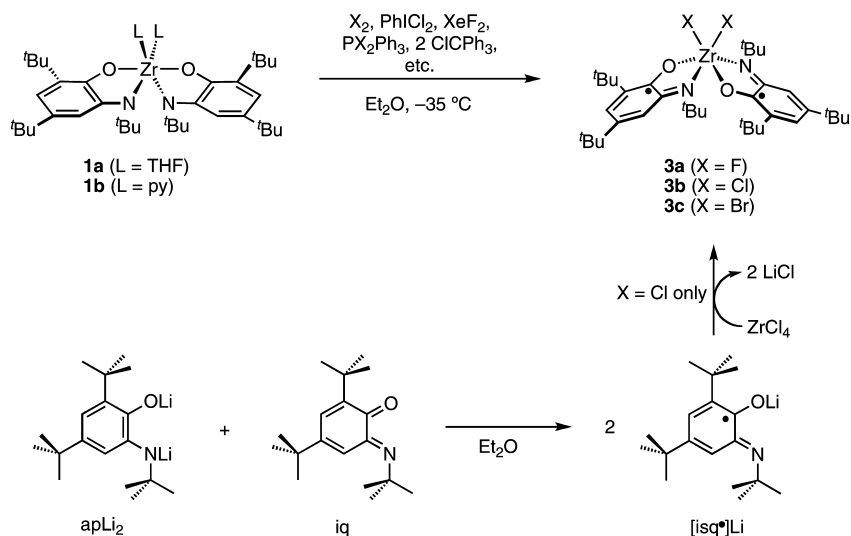
fluoride derivative, ZrF$_2$[isq·]$_2$ (**3a**), was prepared by the reaction of **1b** with XeF$_2$; however, crystalline material suitable for single-crystal X-ray diffraction studies was never obtained. Further oxidation of complexes **3a** and **3b** with another equivalent of halogen led to the formation of free iq and the corresponding zirconium halide salt (eq 1). This result is consistent with recent reports of the bromine oxidation of Cu^{II}[isq·]$_2$ to Cu^{II}Br$_2$[iq]$_2$.[37]
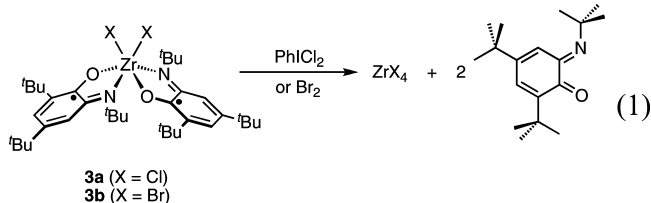
An alternative strategy for the synthesis of **3b** relied on the conproportionation of [ap]$^{2-}$ with its two-electron oxidized derivative, 2,4-di-*tert*-butyl-6-*tert*-butyliminoquinone (iq), to form 2,4-di-*tert*-butyl-6-*tert*-butylimino-semiquinonate ([isq·]$^-$). We have prepared and studied iq, which conproportionates with apH$_2$ to form the first example of a stable, neutral imino-semiquinone radical, [isq·]H.[23] The deprotonated form, [isq·]$^-$, was prepared from an equimolar mixture of [ap]Li$_2$ and iq in ether. Upon addition of ZrCl$_4$ to a cold ether solution of [isq·]Li, the color quickly changed to olive green. After filtration to remove LiCl, **3b** was isolated by cooling the green ether solution of the complex to −35 °C.

To probe further the oxidation reactivity of the Zr[ap]$_2$L$_2$ platform, **1a** and **1b** were reacted with the outer-sphere ferrocenium oxidants. Oxidations of **1a** or **1b** carried out with [Cp$_2$Fe][BPh$_4$] always gave intractable solids that were NMR silent; however, bis(pyridine) adduct **1b** reacted with 2 equiv of [Cp$_2$Fe][PF$_6$] to afford the difluoride **3a**, 2 equiv of C$_5$H$_5$N-PF$_5$ and 2 equiv of ferrocene (eq 2). The latter products were identified by mass spectrometry and by

comparison of ^{1}H NMR spectroscopic data to independently prepared samples. Because of similar solubilities, it was impossible to separate **3a** from the reaction byproducts by recrystallization, though Cp$_2$Fe and C$_5$H$_5$N-PF$_5$ could be removed by sublimation at the expense of a reduced yield of **3a**.
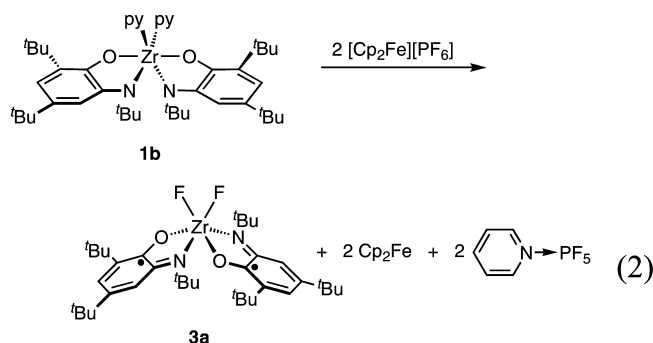
Halogen oxidation reactions of hafnium complex **5** proceeded much like the oxidation reactions of zirconium derivative **1a**. Addition of PhICl$_2$ to yellow solutions of **5** resulted in an immediate color change to dark green. As with the zirconium derivative, maximum yields of crystalline HfCl$_2$[isq·]$_2$ (**6b**) were obtained when reaction mixtures were stored at −35 °C. Similarly, bromine oxidation of **5** afforded the bromide product, HfBr$_2$[isq·]$_2$ (**6c**) in 61% yield. The chloride and bromide derivatives were also generated in good yields using alternative oxidants like *N*-chlorosuccinimide and *N*-bromosuccinimide, respectively. All attempts to generate the fluoride derivative, HfF$_2$[isq·]$_2$ (**6a**), were frustrated by side reactions. While oxidation of the starting metal complex was clearly evident in the observed color changes, crystalline samples of the desired product were never obtained. Moreover, side reactions always led to the formation of hafnium containing byproducts such as HfF(apH)$_3$ (see Supporting Information), formed either by an H-atom abstraction pathway or by reaction with adventitious water.

Halogen oxidations of titanium derivative **4** were unsuccessful in generating oxidative addition products. The

(37) Mukherjee, C.; Weyhermüller, T.; Bothe, E.; Chaudhuri, P. *Inorg. Chem.* **2008**, *47*, 2740–2746.
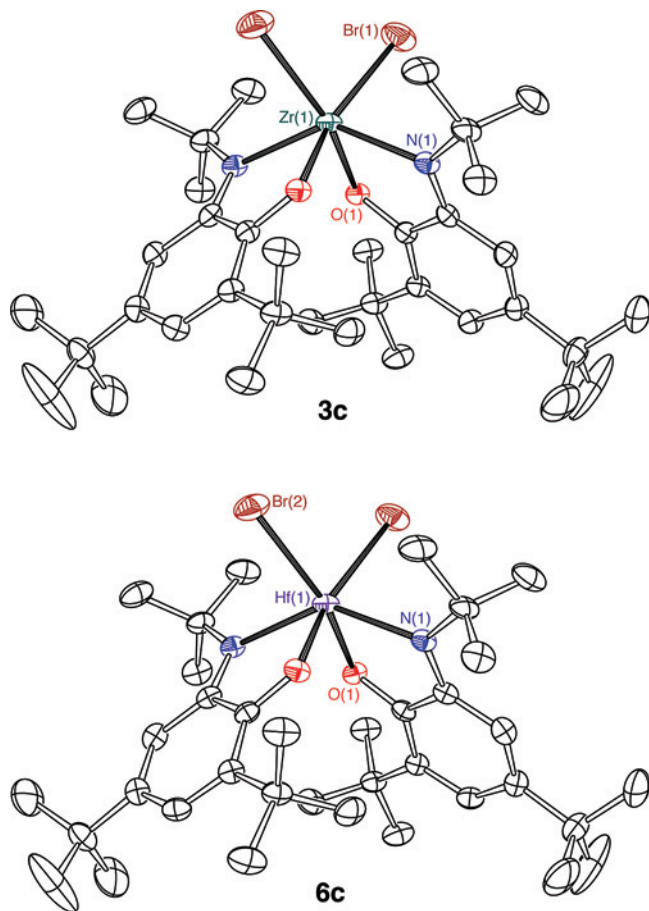
Figure 4. ORTEP diagrams of ZrBr$_2$[isq•]$_2$ (**3c**) and HfBr$_2$[isq•]$_2$ (**6c**). Ellipsoids are drawn at 50% probability and hydrogen atoms have been omitted for clarity.

addition of PhICl$_2$ or Br$_2$ to purple solutions of **4** resulted in a rapid color change to brown; crystalline product was never isolated. Several attempts to isolate a titanium oxidative-addition product yielded only amorphous paramagnetic species that were not characterized fully.

Solid State Structures of MX$_2$[isq•]$_2$ Complexes. Single crystal X-ray diffraction studies were conducted to elucidate the solid-state structures of complexes **3b**, **3c**, **6b**, and **6c**. ORTEP diagrams for two derivatives, **3c** and **6c**, are shown in Figure 4; selected metrical parameters describing the metal coordination spheres of **3b**, **3c**, **6b**, and **6c** can be found in Table 3. All four complexes crystallized in the monoclinic space group *C*2/*c* with the metal ion located on a special position. The metal centers of each compound are six-coordinate, comprising two chelating [isq•]$^-$ ligands (see below) and two monodentate halide ligands. Relative to **1a** and **5**, the core of complexes **3b,c** and **6b,c** is distorted toward trigonal prismatic, with angles between X–O–N trigonal faces of approximately 25°.[38] Bond distances from the metal to the [ap]$^{2-}$ ligand donor atoms are remarkably consistent across the series with the largest observed difference in M–N and M–O distances being only 0.025 Å. The [isq•]$^-$ ligands in **3** and **6** are rearranged relative to the reduced [ap]$^{2-}$ ligands of **1** and **5**. This change is most

(38) For an octahedron the angle should be 60°; for a trigonal prism the angle should be 0°.

evident in the O–M–O angle, which closes from 160° in **1a** and **5** to 93° in **3** and **6**, and in the N–M–N angle, which opens from 104° in **1a** and **5** to 136° in **3** and **6**. The metal–halide distances in **3** and **6** are normal, and there is little difference between the observed Zr–X and Hf–X distances, consistent with the similarity in the metal radius of zirconium(IV) and hafnium(IV) in complexes.[39]

Bond distances within the chelating [isq•]$^-$ ligands provided experimental evidence for the monoanionic ligand oxidation state. As shown in Chart 1, which compares intraligand bond distances from the structures of **1a** and **3b**, the oxidation of both zirconium and hafnium complexes results in significant changes to the ligand bonding framework. Notably, upon oxidation, the Zr–O and Zr–N bond distances increase, while the C–O and C–N bond distances decrease. Whereas the ligand C–C distances in **1a** are consistent with an aromatic phenyl ring, the ligand C–C distances in **3b** show localization of double bond character. Bond distance perturbations like these, which are similar for all of the oxidized zirconium and hafnium complexes reported here, have been used as experimental measures of the ligand oxidation state.[40,41]

Electronic Structure of MX$_2$[isq•]$_2$ Complexes. The isostructural arrangement of the open-shell [isq•]$^-$ ligands in **3b,c** and **6b,c** prompted a comparison of their electronic and magnetic properties in the solid state and in solution. Oxidized complexes **3a–c** and **6b,c** all appear paramagnetic in solution. ^{1}H NMR spectra of these compounds dissolved in C$_6$D$_6$ showed only a single broad resonance at 1.0 ppm at room temperature; cooling these samples to −55 °C did not result in a significant improvement to the NMR spectra. The room-temperature solution magnetic susceptibilities of **3b** and **3c** were determined by Evan's Method measurements. Both complexes showed similar effective magnetic moments, which are given in Table 4.

To further probe the magnetic properties of **3** and **6**, solid-state magnetic susceptibility measurements were conducted in a SQUID magnetometer. Microcrystalline samples of **3b**, **3c** and **6b**, **6c** were examined between 4 and 400 K; the resulting χ_M vs T plots are shown in Figure 5 and the μ_{eff} vs T plots are shown in the Supporting Information.[42] At 4 K the complexes showed an effective magnetic moment approaching zero, but as the temperature was raised, an increase in the effective magnetic moment was observed. At 298 K, solid samples of all four complexes have an effective magnetic moment between 1.26−1.49 μ_B, which is slightly higher than the Evans' Method data obtained for samples in solution. The χ_M vs T plots in Figure 5 show essentially

(39) Holleman, A. F.; Wiberg E. In *Inorganic Chemistry*; Wiberg, N., Aylett, B. J., Eds.; Academic Press: San Diego, CA, 2001; Appendix IV.

(40) Bhattacharya, S.; Gupta, P.; Basuli, F.; Pierpont, C. G. *Inorg. Chem.* **2002**, *41*, 5810–5816.

(41) Chaudhuri, P.; Verani, C. N.; Bill, E.; Bothe, E.; Weyhermüller, T.; Wieghardt, K. *J. Am. Chem. Soc.* **2001**, *123*, 2213–2223.

(42) Magnetic susceptibility measurements of zirconium fluoride derivative **3a** are consistent with the measurements obtained for **3b** and **3c**, suggesting an analogous coordination geometry. Despite this result, we have restricted our discussion of the magnetic data to those complexes that we have structurally characterized by X-ray crystallography.

Table 3. Selected Metrical Data for MX$_2$[isq$^\bullet$]$_2$ (**3b**, M = Zr, X = Cl; **3c**, M = Zr, X = Br; **6b**, M = Hf, X = Cl; **3a**, M = Hf, X = Br)

	ZrCl$_2$[isq$^\bullet$]$_2$ (**3b**)	ZrBr$_2$[isq$^\bullet$]$_2$ (**3c**)	HfCl$_2$[isq$^\bullet$]$_2$ (**6b**)	HfBr$_2$[isq$^\bullet$]$_2$ (**6c**)
		bond lengths/Å		
M−O(1)	2.0811(17)	2.0703(18)	2.067(2)	2.051(2)
M−N(1)	2.247(2)	2.253(2)	2.239(3)	2.231(3)
M−X(1)	2.4753(8)	2.6382(5)	2.4531(11)	2.6227(9)
		bond angles/deg		
O(1)−M−N(1)	72.60(7)	72.68(7)	73.48(10)	73.61(10)
O(1)−M−O(1)′	92.35(9)	93.46(10)	93.03(13)	94.53(10)
N(1)−M−N(1)′	135.22(10)	135.70(11)	136.81(15)	137.06(15)
X(1)−M−X(1)′	89.59(4)	89.32(2)	89.16(6)	89.10(4)
O(1)−M−X(1)	92.48(5)	92.09(5)	92.28(8)	91.67(7)
N(1)−M−X(1)	86.15(6)	85.84(6)	86.05(8)	85.69(8)

Chart 1

Zr(ap)$_2$(THF)$_2$ (**1a**)   ZrCl$_2$(isq)$_2$ (**3a**)
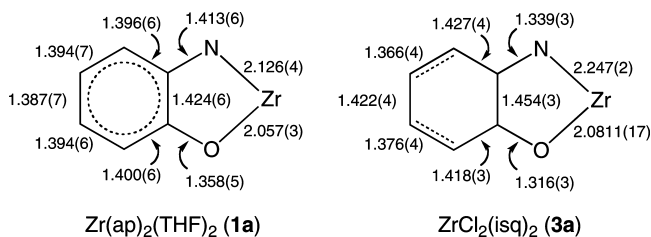
Table 4. Solution and Solid-State Magnetic Data for MX$_2$[isq$^\bullet$]$_2$ (**3b**, M = Zr, X = Cl; **3c**, M = Zr, X = Br; **6b**, M = Hf, X = Cl; **3a**, M = Hf, X = Br)

	solution μ_{eff} (298 K)/μ_B	solid-state μ_{eff} (298 K)/μ_B	TIP/10^{-4} emu
ZrCl$_2$[isq$^\bullet$]$_2$ (**3b**)	0.80	1.32	7.4(7)
ZrBr$_2$[isq$^\bullet$]$_2$ (**3c**)	0.66	1.49	8.4(8)
HfCl$_2$[isq$^\bullet$]$_2$ (**6b**)		1.40	7.9(7)
HfBr$_2$[isq$^\bullet$]$_2$ (**6c**)		1.26	6.7(5)

constant values for χ_M and indicate that the increases in μ_{eff} derive solely from temperature independent paramagnetism (TIP). The TIP values for **3b,c** and **6b,c** are collected in Table 4.

At 298 K, the solution EPR spectra of **3b**, **3c**, **6b**, and **6c** all display a four-line signal centered around 3325 G. The spectrum for **3a** is shown in Figure 6; it is similar to the solution EPR spectrum of the neutral semiquinone, isqH$^\bullet$,[23] but with additional superhyperfine coupling due to the 5/2 nuclear spin of ^{91}Zr. The presence of zirconium superhyperfine coupling in the $\Delta m_s = 1$ transition suggests that the signal does not arise from dissociated [isq$^\bullet$]$^-$, but rather from
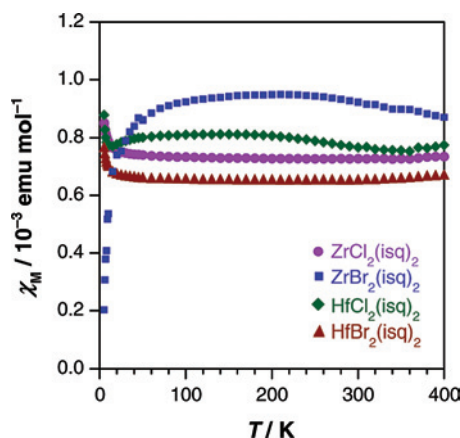
Figure 5. Molar magnetic susceptibility of solid samples of MX$_2$[isq$^\bullet$]$_2$ (**3a**, M = Zr, X = Cl; **3b**, M = Zr, X = Br; **6a**, M = Hf, X = Cl; **6b**, M = Hf, X = Br).

uncorrelated spins within a single molecule. Spin integration measurements were made for a 5.8 M solution of **3b** in THF. At 298 K, the approximate spin concentration was estimated to be 1.9 M or 12%. When the solution of **3b** was cooled to 77 K line broadening was observed. Finally, at temperatures below 60 K, a broad $\Delta m_s = 2$ signal was observed at 1717 G (Figure 6, inset). These results are consistent with a biradical complex displaying antiferromagnetic coupling between the two electrons.[43−45]

As expected for complexes with open-shell ligands, the electronic absorption spectra of **3** and **6** are dominated by strong transitions in the visible region of the spectrum. In both solution and in the solid state, complexes **3** and **6** are dark green. Figure 7 displays the UV−vis spectra for **3b**, **3c**, **6b**, and **6c** in benzene at room temperature. An intense transition at λ_{max} = 789 nm was observed for zirconium dichloride complex **3b**, which red shifts by only 8 nm (65 cm^{-1}) for zirconium dibromide derivative **3c**. The hafnium complexes show similar absorbances that are blue-shifted by about 30 nm (430 cm^{-1}); λ_{max} = 760 nm for hafnium dichloride **6b** and λ_{max} = 765 nm for hafnium dibromide **6c**. Low-energy absorbances such as these are common in metal complexes with two or more open-shell imino-semiquinonate ligands. Typically, these transitions are insensitive to the nature of the central metal ion and can be attributed to allowed ligand-to-ligand charge transfer (LLCT) transitions.[41]

Discussion

"Oxidative Addition" Reactions. One way to understand the stability of oxidative-addition products **3** and **6** is to examine the electrochemical properties of the halogen oxidant and the redox-active amidophenolate ligand. In our hands, clean, reversible electrochemical measurements for zirconium complexes **1** and **3** and hafnium complexes **5** and **6** could not be obtained. We suspect this inability results from bond-making and bond-breaking processes that occur upon oxidation or reduction of the complexes. For example, electrochemical oxidation of **1a** or **1b** would generate a zirconium radical cation species that would be expected to

(43) Roques, N.; Gerbier, P.; Schatzschneider, U.; Sutter, J.; Guionneau, P.; Vidal-Gancedo, J.; Veciana, J.; Rentschler, E.; Guerin, C. *Chem. Eur. J.* **2006**, *12*, 5547–5562.

(44) Roques, N.; Gerbier, P.; Sutter, J.; Guionneau, P.; Luneau, D.; Guerin, C. *Organometallics* **2003**, *22*, 4833–4835.

(45) Rajca, A.; Rajca, S.; Wongsriratanakul, J. *Chem. Commun.* **2000**, 1021–1022.
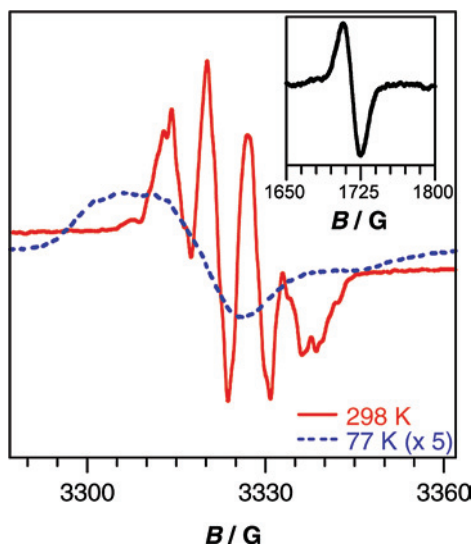
Figure 6. EPR spectrum in the $\Delta m_s = 1$ region for a solution of $ZrCl_2[isq\cdot]_2$ (**3a**) dissolved in toluene at 298 K (red) and 77 K (blue) and in the $\Delta m_s = 2$ region at 60 K (inset).
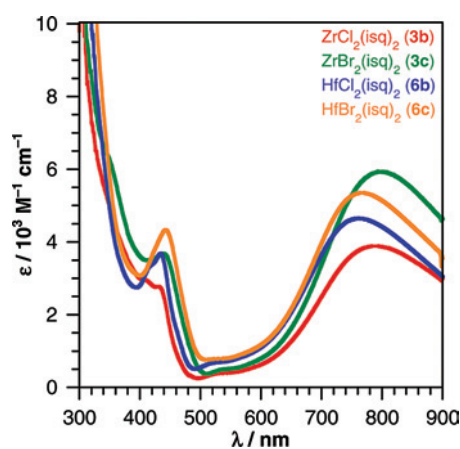
Figure 7. UV−vis absorption spectra of $MX_2[isq\cdot]_2$ (**3a**, M = Zr, X = Cl, red; **3b**, M = Zr, X = Br, green; **6a**, M = Hf, X = Cl, blue; **6b**, M = Hf, X = Br, orange) in benzene.

add halides according to the $[Cp_2Fe][PF_6]$ oxidations reported above. Similarly, electrochemical reduction of **5** would give a dihalide zirconium radical anion, which would be expected to rapidly lose a halide in solution.[46] On the other hand, halogen oxidations of **1a** and **5** proceed smoothly and can be used to benchmark the reactivity of these complexes. Oxidations of **1a** and **5** with halogens such as Cl_2 and Br_2, or with halogen delivery reagents such as XeF_2, $PhICl_2$ or Ph_3PBr_2 afford the corresponding halide products **3** and **6**. Attempts to oxidize either **1a** or **5** with iodine did not lead to the formation of the analogous iodide products, $MI_2[isq\cdot]_2$ (M = Zr or Hf). The $[isqH\cdot]^0/[apH]^-$ reduction potential ($E^{\circ\prime} = +0.06$ V vs $Cp_2Fe^{+/0}$)[23,47] provides an indication of how easily complexes **1a** and **5** can be oxidized. Nonaqueous halogen reduction potentials[48] suggest that chlorine should readily oxidize **1a** and **5**, and that bromine is a closely

matched oxidant for the apH_2 ligand. On the other hand, it can be estimated that iodine is too weak of an oxidant (by approximately 200 mV) to oxidize the amidophenolate ligand.[47]

The clean formation of **3a** by the ferrocenium oxidation of **1b** is surprising given the value of the $[isqH\cdot]^0/[apH]^-$ reduction potential, but is consistent with the ferrocenium-based oxidation of $Zr[ap]_2Ph_2^{2-}$ that leads to C−C reductive elimination.[49] As shown in eq 1, treatment of **1b** with two equivalents of $[Cp_2Fe][PF_6]$, led to the formation of **3a**. While many ferrocenium salts initiated the oxidation of zirconium complexes **1a** and **1b** (as indicated by color changes to dark green), a tractable two-electron oxidized product was isolated only for reactions between **1b** and $[Cp_2Fe][PF_6]$. The relative oxidation potentials of the apH_2 ligand and Cp_2Fe^+ suggest that this oxidation reaction should be disfavored by nearly 60 mV;[47] however, in the case of eq 2, the formation of strong zirconium-fluoride interactions may work to drive the oxidative addition reaction forward. A stepwise mechanism for the reaction of **1b** with $[Cp_2Fe][PF_6]$ is proposed in eqs 3−7. One-electron oxidation of **1b** would give a zirconium cation (eq 4), which would likely be Lewis acidic enough to abstract fluoride from a PF_6^- anion (eq 5). A second one-electron oxidation (eq 6), followed by fluoride transfer (eq 7), would give the observed products.

$$2Cp_2Fe^+ + 2e^- \rightarrow 2Cp_2Fe \qquad (3)$$

$$Zr[ap]_2(py)_2 \rightarrow Zr[isq\cdot][ap](py)_2^+ + e^- \qquad (4)$$

$$Zr[isq\cdot][ap](py)_2^+ + PF_6^- \rightarrow ZrF[isq\cdot][ap](py) + py\text{-}PF_5 \qquad (5)$$

$$ZrF[isq\cdot][ap](py) \rightarrow ZrF[isq\cdot]2(py)^+ + e^- \qquad (6)$$

$$ZrF[isq\cdot]_2(py)^+ + PF_6^- \rightarrow ZrF_2[isq\cdot]_2 + py\text{-}PF_5 \qquad (7)$$
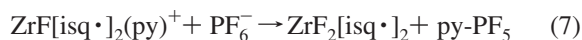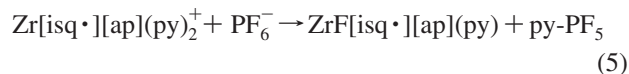
In contrast to the facile formation of zirconium and hafnium oxidative addition products, analogous products with titanium were not isolable. Addition of fluorine-, chlorine-, or bromine-based reagents to **4** resulted in color changes attributable to oxidation, yet tractable oxidative-addition products were not obtained. The instability of a $TiX_2[isq\cdot]_2$ oxidative addition product might stem from the accessibility of the Ti(III) oxidation state.[50] According to eq 8, intramolecular electron transfer from an $[isq\cdot]^-$ ligand to the titanium center of a $TiX_2[isq\cdot]_2$ species would provide a mechanism for disproportionation of the two iminosemiquinonate ligands to an aminophenolate ligand and a free iminoquinone.[51] This type of redox isomerism, or valence tautomerism, has been observed for manganese and cobalt complexes with catecholate-type ligands.[52,53] The observation of free iminoquinone during halogen oxidations of **4** is consistent with the

(46) Blackmore, K. J.; Ziller, J. W.; Heyduk, A. F. *Inorg. Chem.* **2008**, *47*, 265–273.
(47) This value is based on the $[isqH\cdot]^0/[apH]^-$ reduction potential rather than the potential for the metallated ligand.
(48) Connelly, N. G.; Geiger, W. E. *Chem. Rev.* **1996**, *96*, 877–910.

(49) Haneline, M. R.; Heyduk, A. F. *J. Am. Chem. Soc.* **2006**, *128*, 8410–8411.
(50) Greenwood, N. N.; Earnshaw, A. *Chemistry of the Elements*; Butterworth-Heinemann: Oxford, 1997; pp 969−971.
(51) Cass, M. E.; Pierpont, C. G. *Inorg. Chem.* **1986**, *25*, 123–125.
(52) Hendrickson, D. N.; Pierpont, C. G. *Top. Curr. Chem.* **2004**, *234*, 63–95.
(53) Pierpont, C. G. *Coord. Chem. Rev.* **2001**, *216−217*, 99–125.

reactivity proposed in eq 8. All efforts to isolate and characterize a coordinatively unsaturated species like TiX$_2$[ap] of eq 8 were unsuccessful; however, analogous titanium complexes with *N,N′*-disubstituted phenylenediamide-type ligands have been reported.[54,55]

(8)
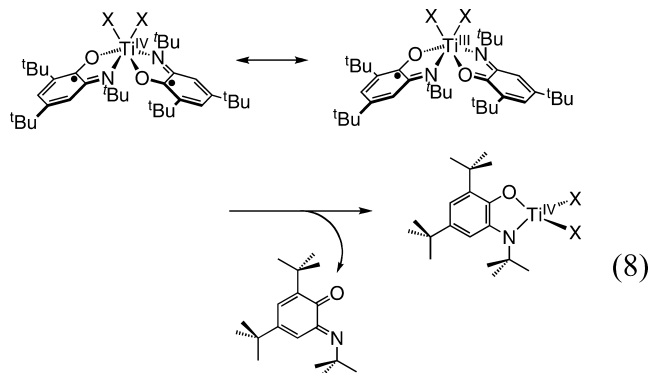
The importance of the titanium(III) oxidation state can be further probed by comparing the electronic absorbance spectra of **4** with the zirconium (**1a**) and hafnium (**5a**) derivatives. Complexes **1a**, **4**, and **5** form an isostructural series of the [ap]$^{2-}$ ligand in which only the Group IV metal ion varies. In the solid state, **1a** and **5** are bright yellow and tan, respectively, but give yellow solutions when dissolved in both coordinating and noncoordinating solvents. In comparison, complex **4** is dark purple in the solid state and crystals of **4** dissolved in benzene gave a deep red-purple solution. As shown in Figure 2, this color derives from a ligand-to-metal charge transfer absorbance at 371 nm that extends out well into the visible portion of the spectrum. The energy of this band is consistent with a smaller gap between the filled redox-active orbitals of the [ap]$^{2-}$ ligands and the empty titanium *d* orbitals, which would facilitate the redox isomerism proposed in eq 8.

Electronic Structure of MX$_2$[isq•]$_2$ Complexes. As we have previously reported,[20] complex **3b** and its congeners adopt a singlet diradical ground state. According to X-ray crystallography data for the products, the oxidative addition of halogens to **1a** and **5** leads to products in which one electron from each [ap]$^{2-}$ ligand is transferred to the incoming halogen oxidant. As a result, each redox-active ligand in the oxidative-addition products can be described as an open-shell imino-semiquinonate radical, [isq•]$^-$. Two [isq•]$^-$ ligands in a single molecule can couple either with opposite spins to give a singlet ($S = 0$) ground-state or with parallel spins to give a triplet ($S = 1$) ground state. Solution EPR spectra of **3b** are consistent with the biradical formulation. At 298 K, an EPR signal, showing superhyperfine coupling to the zirconium center, is observed at $g = 2.01$, consistent with a $\Delta m_s = 1$ transition of a single uncorrelated electron. Upon cooling, this signal broadens and decreases in intensity. A $\Delta m_s = 2$ transition was also observed in the low-temperature solution EPR spectrum of **3b** at 1717 G.

(54) Ketterer, N. A.; Ziller, J. W.; Rheingold, A. L.; Heyduk, A. F. *Organometallics* **2007**, *26*, 5330–5338.
(55) Aoyagi, K.; Gantzel, P. K.; Kalai, K.; Tilley, T. D. *Organometallics* **1996**, *15*, 923–927.
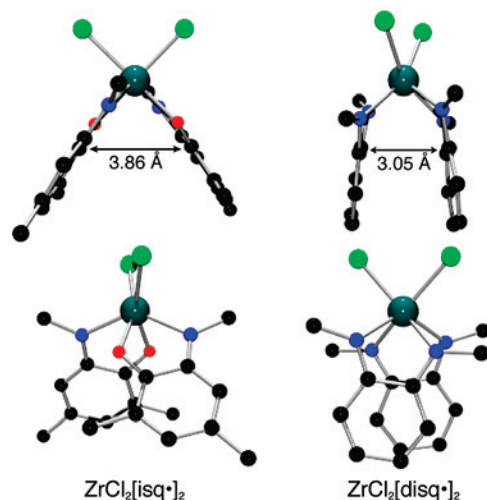
Figure 8. Geometry comparison between ZrCl$_2$[isq•]$_2$ (**3b**) and ZrCl$_2$[disq•]$_2$. In the case of ZrCl$_2$[isq•]$_2$, the distance was measured between the closest carbon atoms of the phenyl ring (bound to O). In the case of ZrCl$_2$[disq•]$_2$, the distance was measured between the midpoints of the C1–C2 bond.

These EPR features are consistent with those observed for other transition metal complexes with ligand-localized radicals and a singlet ground state.[43–45]

The solid-state magnetic susceptibility studies summarized in Figure 5 and in the Supporting Information are consistent with the solution EPR data and show that the ground-state of zirconium derivatives **3b** and **3c**, as well as hafnium derivatives **6b** and **6c**, is the singlet. As solid samples of these complexes are warmed to room temperature, the effective magnetic moment increases but never achieves the spin-only value for two unpaired electrons (spin-only $\mu_{\text{eff}} = 2.83 \ \mu_B$). As is clearly seen in Figure 5, this behavior is strictly a result of temperature-independent paramagnetism. Recently, we reported similar electronic behavior for complexes of the formulation ZrX$_2$[disq•]$_2$ (X = Cl, Br, I; [disq•]$^-$ = *N,N′*-di(*neo*)pentyl-*ortho*-diimino-semiquinonate). As shown in Figure 8, structural flexibility in the [disq•]$^-$ ligands allowed the formation of a π-stacked, bonding interaction that eliminated diradical character in the ZrX$_2$[disq•]$_2$ complexes. As a result, the ZrX$_2$[disq•]$_2$ complexes have a closed-shell singlet ground state. No $\Delta m_s = 1$ EPR transition was observed at any temperature for the ZrX$_2$[disq•]$_2$ complexes. In contrast, in complexes **3a–c** the [isq•]$^-$ ligands are not close enough to have a strong through-space interaction and as such, these complexes have significant biradical character in the ground state, with the $S = 0$ spin state arising from antiferromagnetic interactions through the *d*^{0} metal centers.

The $S = 0$ ground-state of complexes **3** and **6** is somewhat surprising in light of previous studies on coordination complexes of metals with empty valence shells and multiple radical semiquinonate ligands. Titanium(IV), germanium(IV) and tin(IV) complexes of the formulation M^{IV}[Cat-N-SQ•]$_2$ ([Cat-N-SQ•]$^-$ = 3,5-di-*tert*-butyl-l,2-semiquinonato-(2-hydroxy-3,5-di-*tert*-butylphenyl)imine) show ferromagnetic coupling between the ligand-based radicals leading to an *S*

= 1 grounds state.[56] Similarly, a $S = 3/2$ ground-state has been reported in gallium(III) and aluminum(III) complexes of 3,5-di-*tert*-butyl-1,2-semiquinonate, $M^{III}(SQ \cdot)_3$, arising from weak ferromagnetic interactions.[57,58] More recently, gallium(III) tris(arylimino-semiquinonate) derivatives have been found to show antiferromagnetic coupling and $S = 1/2$ ground states with the strength of the antiferromagnetic coupling increasing with increasing Hammett donor ability of the substituents on the arylimino group.[59] If electron density on the nitrogen of the redox-active ligand is a key property leading to antiferromagnetic coupling, it stands to reason the *tert*-butylimino group of the [isq$\cdot$]$^-$ ligands in **3** and **6**, would readily facilitate such an interaction. On the other hand, another factor influencing the electron−electron communications in **3** and **6** might be the overall coordination geometry at the metal center. In the case of $M^{IV}[Cat-N-SQ\cdot]_2$

and $M^{III}[SQ\cdot]_3$ complexes, a pseudo-octahedral or trigonal antiprismatic geometry was observed in the solid state. This geometry places the singly occupied π orbitals of each redox active ligand in the $M^{IV}[Cat-N-SQ\cdot]_2$ and $M^{III}[SQ\cdot]_3$ complexes perpendicular to each other so they must interact with orthogonal metal-based d orbitals. In the case of **3** and **6**, the solid-state structures are distorted toward trigonal prismatic geometry, and as such the singly occupied π orbitals are no longer perpendicular, allowing them to interact with the same metal-based d orbital.

Supporting Information Available: χ vs T plots for **3b**, **3c**, **6b**, and **6c** and X-ray diffraction data for complexes **2**, **3c**, **4**, **5**, **6b**, and **6c** (PDF and CIF). This information is available free of charge via the Internet at http://pubs.acs.org.

IC801127R

(56) Bruni, S.; Caneschi, A.; Cariati, F.; Delfs, C.; Dei, A.; Gatteschi, D. *J. Am. Chem. Soc.* **1994**, *116*, 1388–1394.
(57) Adams, D. M.; Rheingold, A. L.; Dei, A.; Hendrickson, D. N. *Angew. Chem., Int. Ed. Engl.* **1993**, *32*, 391–392.
(58) Lange, C. W.; Conklin, B. J.; Pierpont, C. G. *Inorg. Chem.* **1994**, *33*, 1276–1283.
(59) Chaudhuri, P.; Wagner, R.; Pieper, U.; Biswas, B.; Weyhermüller, T. *Dalton Trans.* **2008**, 1286–1288.